Ionic Liquids with Symmetric Isoelectronic Diether Tails: Bulk and Vacuum-Liquid Interfacial Structures

Journal:	*The Journal of Physical Chemistry*
Manuscript ID	jp-2016-09148z.R1
Manuscript Type:	Article
Date Submitted by the Author:	n/a
Complete List of Authors:	Hettige, Jeevapani; University of Iowa, Chemistry Amith, Weththasinghage; The University of Iowa, Department of Chemistry Castner, Edward; Rutgers, The State University of New Jersey, Department of Chemistry and Chemical Biology Margulis, Claudio; The University of Iowa, Department of Chemistry

Ionic Liquids with Symmetric Isoelectronic Diether Tails: Bulk and Vacuum-Liquid Interfacial Structures

Jeevapani J. Hettige,[†] Weththasinghage D. Amith,[†] Edward W. Castner Jr.,[‡] and Claudio J. Margulis[*,†]

†*Department of Chemistry, University of Iowa, Iowa City, IA 52242, USA*

‡*Department of Chemistry and Chemical Biology, Rutgers, The State University of New Jersey, Piscataway, New Jersey 08854, USA*

E-mail: claudio-margulis@uiowa.edu

Abstract

The behavior in the bulk and at interfaces of biphilic ionic liquids in which either the cation or anion possesses moderately long alkyl tails is to a significant degree well understood. Less clear is what happens when both the cation and anion possess tails that are not apolar such as in the case of ether functionalities. The current article discusses the structural characteristics of C2OC2OC2-mim$^+$/C2OC2OC2-OSO$_3^-$ in the bulk and at the vacuum interface. We find that the vacuum interface affects only the nanometer length scale. This is in contrast to what we have recently found in (*J. Phys. Chem. Lett.*, 2016, 7 (19), 3785-3790) for isoelectronic C[8]-mim$^+$/C[8]-OSO$_3^-$, where the interface effect is long ranged. Interestingly, ions with the diether tail functionality still favor the tail-outwards orientation at the vacuum interface and the bulk phase preserves the alternation between charged networks and tails that is commonly observed for biphilic ionic liquids. However, such alternation is less well defined and results in a significantly diminished first sharp diffraction peak in the bulk liquid structure function.

Introduction

A significant portion of the ionic liquid (IL) literature describes systems in which cations have a polar head and an apolar tail and anions are in general smaller, more or less symmetrically charged and with no significant apolar components.[1–19] All of these ILs fall into what one could call the biphilic paradigm, where either the anion of the cation is strongly amphiphilic, having polar head groups and apolar tails. Less well studied are systems in which anions and cations have similar polar/apolar characteristics. The last few years have brought significant interest to systems in which the cation contains tails that are ether functionalized.[20–27] This is because such systems have been shown to be of low viscosity[21,28,29] and advantageous for electrochemical or energy applications in general.[30–38]

The current computational study focuses on C2OC2OC2-mim$^+$/C2OC2OC2-OSO$_3^-$ (shown

in Fig. 1) in which tails are polar, have identical functionalities, and identical length. We want to contrast the current work on bulk and interfacial properties of C2OC2OC2-mim$^+$/C2OC2OC2-OSO$_3^-$, with prior results on C[8]-mim$^+$/C[8]-OSO$_3^-$,[39] where cationic and anionic tails are identical and apolar. All simulation data on C[8]-mim$^+$/C[8]-OSO$_3^-$ used in this work is published as reference 39.

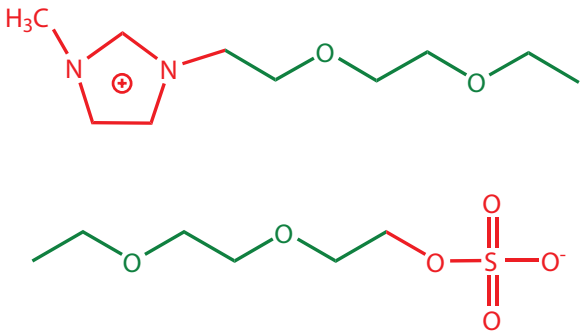

Figure 1: Chemical structure of C2OC2OC2-mim$^+$/C2OC2OC2-OSO$_3^-$.

We recently observed that in the case of C[8]-mim$^+$/C[8]-OSO$_3^-$, bulk and slab configurations in contact with vacuum are very different.[39] The bulk liquid morphology is sponge-like, with a disordered but apparently continuous charge network intercalating the apolar liquid subcomponent. Instead, the slab configuration forms a repetitive lamella. Such condensed phase morphological transformations can potentially be very attractive for energy applications particularly for capacitors. To the best of our knowledge, the behavior in the bulk and at interfaces of the isoelectronic C2OC2OC2-mim$^+$/C2OC2OC2-OSO$_3^-$ is yet unstudied. Do ions with symmetrical tails that break the polar-apolar biphilic paradigm modulate intermediate range order? How deep into the IL does the effect of the interface persist?

We know from our prior work[25,27] and that of others[24,26] that tails of ions with ether functionalities tend to curl towards the charged head. This curling combined with the solvation by charge of the ether functionality has been shown in other systems to disrupts charged head-tail alternation and hence diminish the intensity of the X-ray prepeak.[25–27] In the case of C2OC2OC2-mim$^+$/C2OC2OC2-OSO$_3^-$, where both cationic and anionic tails are

moderately long, the extent to which charged heads and tails alternation may persist in the bulk and at the interface is unclear. Does the liquid still show a well defined charge network that forms a separate nanoscale domain with the apolar tail subcomponents? This leads next to the question: what is the behavior of the diether functionalized tails at the vacuum interface?

Computational and Theoretical Methods

The protocol used for the equilibration of the bulk and vacuum-IL interface of C2OC2OC2-mim$^+$/C2OC2OC2-OSO$_3^-$ is given below. All protocols and data for C[8]-mim$^+$/C[8]-OSO$_3^-$ are from reference 39.

Bulk IL simulations: The bulk phase of C2OC2OC2-mim$^+$/C2OC2OC2-OSO$_3^-$ was modeled using a simulation box containing 1000 pairs. All molecular dynamics simulations were performed using the GROMACS[40] package using a combination of parameters derived from the well-established Canongia-Lopes & Pádua[41] (CL&P) potentials as well as references 42–46. Dihedral parameters that included ether functionalities were taken from citations[40,44,45] as described in reference 25. Charges (Tables S.1 and S.2 in the SI) were not available from literature and were fitted using the CHelpG method at the DFT level (B3LYP) and using the 6-311++G** basis set in Gaussian09.[47] For C[8]-mim$^+$/C[8]-OSO$_3^-$ and C2OC2OC2-mim$^+$/C2OC2OC2-OSO$_3^-$, figures S.2 and S.3 in the SI display a comparison of relevant dihedral distributions in tail components resulting from our choice of force field parameters.

As done in our previous studies,[12,13,25,48–50] the system was first equilibrated for ∼2.5 ns by scaling the atomic charges from 0% to 100%, and raising and lowering the pressure. Then a simulated annealing protocol was followed for 4 ns by raising the system temperature from 300 K to 500 K and then bringing the temperature back to the desired target temperature of 425 K. After the simulated annealing procedure, the system was equilibrated in the NPT ensemble for 8 ns at 425 K and 1 bar pressure. During this final stage of equilibration, the

Nose-Hoover[51,52] thermostat and Parrinello-Rahman[53] barostat were utilized to control the temperature and pressure of the system. The Leap-Frog algorithm was used as the integrator for the equations of motions, with a time step of 1 fs. Coulomb and Lennard-Jones cut offs were set to 1.5 nm, while the Particle Mesh Ewald (PME)[54,55] method (EW3D) was used to calculate electrostatic interactions with an interpolation order of 6 and Fourier grid spacing of 0.8 Å. The final dimensions of the thoroughly equilibrated box were 8.52391 x 8.52391 x 8.52391 nm^3. Vacuum-IL simulations: For the vacuum-IL simulation, the thoroughly equilibrated bulk C2OC2OC2-mim^+/C2OC2OC2-OSO_3^- was further equilibrated in the NVT ensemble for 5 ns. The simulation box was then placed at the center of a tetragonal supercell of dimensions of 8.52391 x 8.52391 x 34.09564 nm^3. The electrostatic interactions during the vacuum-IL simulation were calculated using the PME method along with the Yeh-Berkowitz[56] correction (EW3DC).[57] The system was then further equilibrated in the NVT ensemble for 5 ns, followed by 8 ns of simulated annealing in which the temperature of the system was ramped up to 725 K and brought back to 425 K. Finally, once at target temperature, the system was further simulated in the NVT ensemble for at least 100 ns. The final 16 ns of the fully equilibrated run were utilized for structural analysis. For the purpose of partitioning the structure function into subcomponents, the cationic head group was defined to include the ring, methyl group, and up to the second methylene group in the diether chain. In the case of the anion, the head group was defined to include up to the first methylene group. These definitions were chosen to match those for C[8]-mim^+/C[8]-OSO_3^- in reference 39 as they properly define the charged subcomponents for that system. Notice that this is not the same as the color-coding in Figs. 1, 3 and S.4 in the SI which was chosen for pictorial purposes.

Results and Discussion

We first compare the bulk liquid structure functions $S(q)$ for C2OC2OC2-mim$^+$/C2OC2OC2-OSO$_3^-$ and C[8]-mim$^+$/C[8]-OSO$_3^-$. In Fig. 2(a), two characteristic peaks can be observed in the $S(q)$ for both systems. The broad peak in $S(q)$ near $q = 1.4$ Å^{-1} is due to many intramolecular and close range intermolecular interactions; this is what we have defined in prior articles as the adjacency peak.[49,50,58] The peak at low q is what is commonly called a prepeak (or first sharp diffraction peak) and is due to alternation on the nanoscale. In the case of typical biphilic ionic liquids the prepeak is linked to polar-apolar alternation. Two salient points must be explored. First for both liquids the charge alternation peak (at around $q = 1$ Å^{-1}) is mostly eliminated. Second, the prepeak is significantly more pronounced in the case of C[8]-mim$^+$/C[8]-OSO$_3^-$. For C[8]-mim$^+$/C[8]-OSO$_3^-$ and C2OC2OC2-mim$^+$/C2OC2OC2-OSO$_3^-$, Figures S.1 (a) and S.1 (b) in the supporting information show selected partial subcomponents of $S(q)$. These two plots clearly prove that the charge alternation peak is missing only due to almost complete cancellations of same-type and opposite-type interactions and not because charge alternation symmetry is absent in any of the two systems. We have explained in prior work that this almost perfect cancellation phenomenon is common.[48,59] What is most interesting is that whereas the amplitude in S.1 (a) and S.1 (b) of charge alternation subcomponents in the structure function $S(q)$ slightly below $q = 1$ Å^{-1} is of the same order of magnitude –both liquids form charge alternation networks– the polar contribution to the prepeak is very different. The difference in the prepeak region is best appreciated from Fig. 2(b) where head-head, tail-tail and head-tail subcomponents of $S(q)$ are displayed for the two ILs. In this figure we see that polar-apolar alternation for C[8]-mim$^+$/C[8]-OSO$_3^-$, gives rise to two peaks and one antipeak at smaller q values (indicating larger domains) than the same type of alternation in the case of C2OC2OC2-mim$^+$/C2OC2OC2-OSO$_3^-$. When peaks and antipeaks are compared in Fig. 2(b), intensities are larger by an order of magnitude in the case of C[8]-mim$^+$/C[8]-OSO$_3^-$. Consistent with previous literature[25,26] for systems with cationic tails containing ether groups, Fig 2(b) shows that different degrees of

curling and the moderately polar nature of these functionalities significantly diminishes but does not completely eliminate the charge network-tail alternation symmetry.

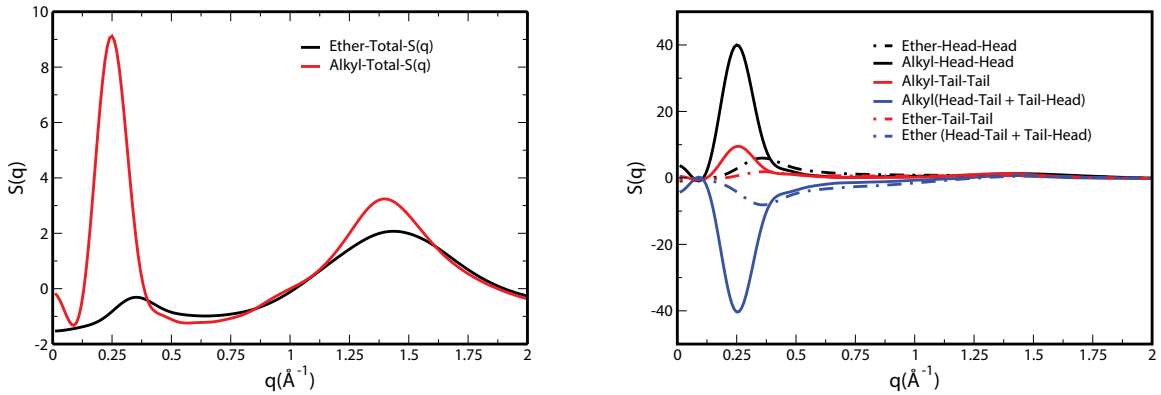

(a) (b)

Figure 2: (a) Total structure function, $S(q)$ for the two systems studied and (b) head-head, tail-tail and head-tail+tail-head subcomponents of $S(q)$. For biphilic ILs this corresponds to the polarity partitioning of $S(q)$ described in references 48, 59 and 12.

Fig. 3 shows snapshots of C2OC2OC2-mim$^+$/C2OC2OC2-OSO$_3^-$ in the bulk and at the IL-vacuum interface in the slab configuration. Figure S.4 in the SI shows the same information but for the case of C[8]-mim$^+$/C[8]-OSO$_3^-$, (please see also Fig. 6 in reference 39). As we have previously noted in reference 39, the bulk phase in the case of C[8]-mim$^+$/C[8]-OSO$_3^-$ (Fig. S.4 (a)) can be described as sponge-like, where a continuous but disordered network of charge intercalates with the apolar subcomponent. The periodicity of the separation between charged regions (intercalated by tails) is well defined as can be appreciated from the intense prepeak in Fig. 2(a) and visually from Fig. S.4 (a). In the case of C2OC2OC2-mim$^+$/C2OC2OC2-OSO$_3^-$, in Fig. 3 (a) we can also visually distinguish areas of charge alternation. However, as was discussed previously for systems in which only the cation has ether functionalities,[25,26] the separation between alternating charge strings and tail regions is not very well defined and charge is more homogeneously distributed. This results in a much smaller prepeak in $S(q)$ with a concomitant decrease in the partial subcomponents of $S(q)$ at the prepeak region in Fig. 2(b).

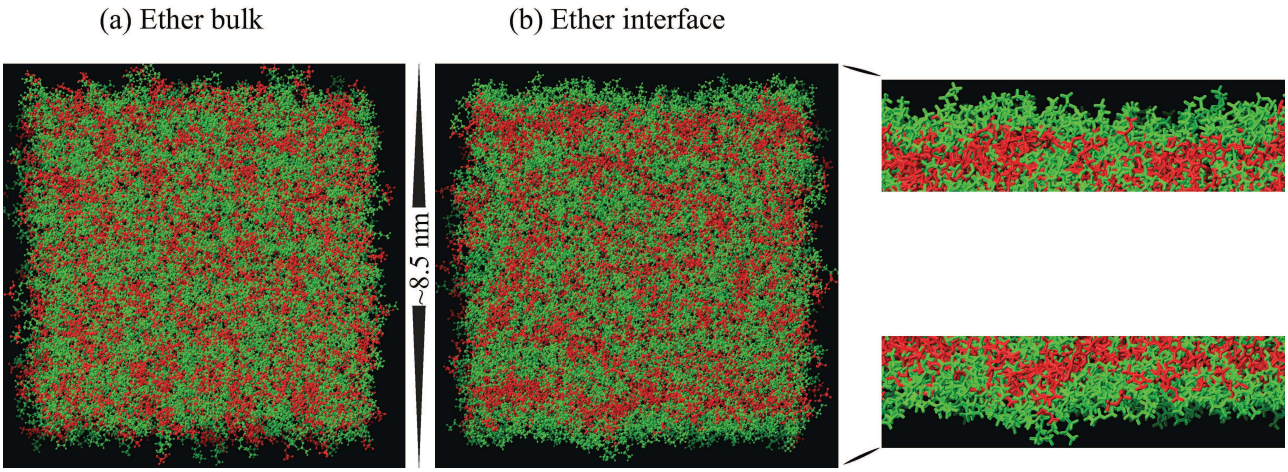

Figure 3: Snapshots of bulk and slab configurations for C2OC2OC2-mim$^+$/C2OC2OC2-OSO_3^-. Inset on the right side shows expanded versions of the the two interfacial regions. The color code follows the same convention as in Fig. 1. Only the immediate liquid vicinity of the interface is affected in the case of C2OC2OC2-mim$^+$/C2OC2OC2-OSO_3^-. This should be contrasted with Fig. S.4 in the SI and Fig. 6 in reference 39 which show that the effect of the interface is long-ranged in the case of C[8]-mim$^+$/C[8]-OSO_3^-.

Perhaps what is most interesting is the situation at the liquid vacuum interface in the slab configuration. As can be seen from Fig. S.4 (b), for C[8]-mim$^+$/C[8]-OSO_3^- changes are dramatic when compared to the bulk (Fig. S.4 (a)). A lamellar phase propagates across the approximately 9 nm slab. The effect of the interface is long ranged, as we have described in reference 39. As can be appreciated from Fig. 3 (b), the opposite is true for the isoelectronic diether functionalized analog where surface induced order is only observed in the vicinity of the interface. Figure 3 (b) clearly shows that ether containing tails are preferentially localized at the vacuum interface, and that a charge layer parallel to the vacuum interface is formed. However, the interface does not induce patterning of the liquid beyond its immediate vicinity, in contrast to what occurs in the case of C[8]-mim$^+$/C[8]-OSO_3^-. Insets on the right side of Fig. 3 highlight the shorter ranged organization in the case of C2OC2OC2-mim$^+$/C2OC2OC2-OSO_3^-.

The statistical conformations of polyethylene oxide (PEO) have been previously studied.[60,61] In particular, our group and others[24–27] have discussed how curling affects intermediate range order for different ILs in which cationic tails contain ether functionalities. To

explore the effect of diether functionalities in the context of interfaces, Fig. 4 shows (i) for cations, the Z-dependent average distance between the imidazolium nitrogen connected to the longer diether (alkyl) tail and the terminal tail carbon and (ii) for anions, the distance between the sulfonyl oxygen connected to the diether (alkyl) tail and terminal tail carbon. As is to be expected, because of tail kinks and curling in the case of the ether containing ions,

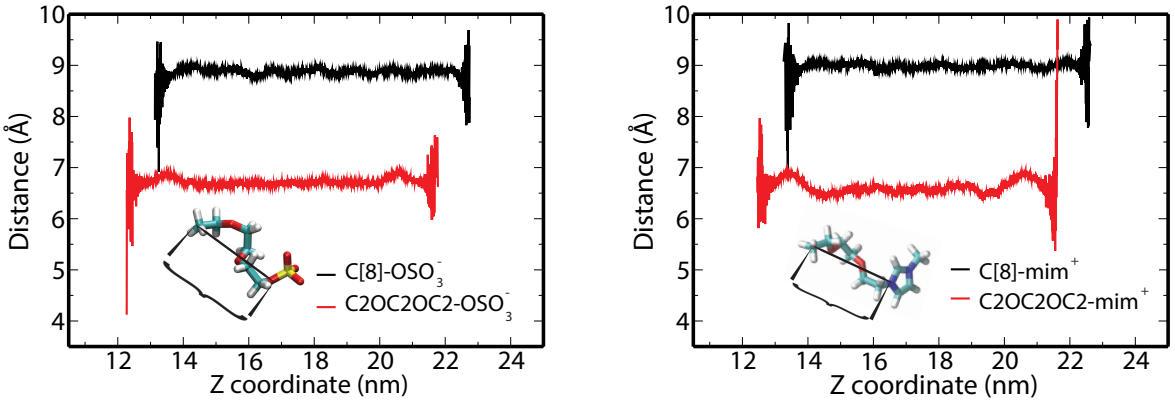

(a) (b)

Figure 4: Z-dependent distance between imidazolium nitrogen (cation)/ sulfonyl oxygen (anion) and terminal carbon atom in the tail for (a)C2OC2OC2-OSO_3^- and C[8]-OSO_3^-, (b)C2OC2OC2-mim $^+$ and C[8]-mim$^+$. This distance is consistently smaller both for anions and cations in the case of diether containing tails because of kinks and curling. Notice the expansion of the diether tails in the proximity of the interface. (Large oscillations at the edges are due to low number count and poor statistics)

distances are smaller when compared to the ions with alkyl tails. Interestingly, when ether functionalized tails meet the vacuum interface, there is a slight increase in this separation. In other words tails are slightly less curled at the interface. Fig. 5 shows the projection of the vector connecting the imidazolium nitrogen (cation)/ sulfonyl oxygen (anion) and the terminal carbon onto the Z unit vector as a function of Z across the slab. Comparing of Figs. 4 and 5 reveals that both C[8]-mim$^+$/C[8]-OSO_3^- and C2OC2OC2-mim$^+$/C2OC2OC2-OSO_3^- have tails mostly pointing towards the vacuum at each interface. In the case of the alkyl tails, it is almost the full length of the vector that projects onto the Z axis. Tails in C2OC2OC2-mim$^+$/C2OC2OC2-OSO_3^- also point towards the vaccum interfaces but are

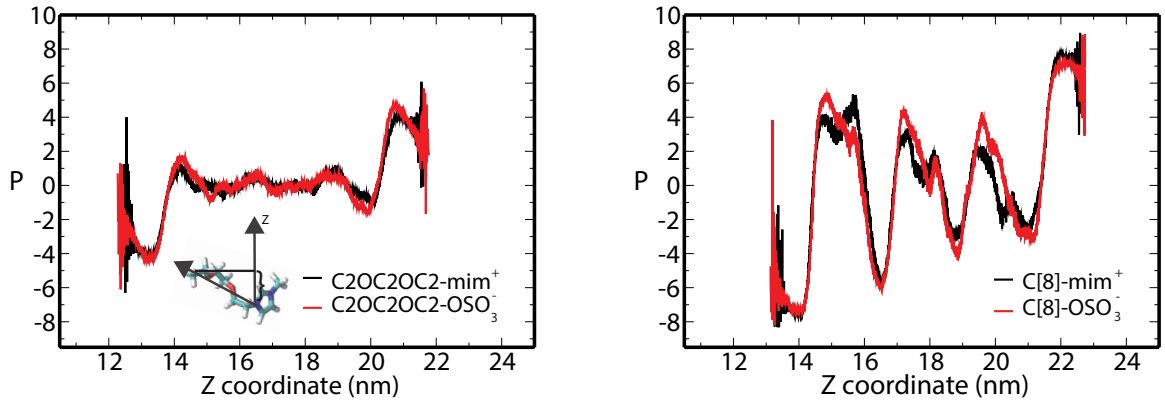

(a) (b)

Figure 5: Z-dependent average projection of the vector between imidazolium nitrogen (cation)/ sulfonyl oxygen (anion) and terminal carbon atom in the tail and a unit vector along Z perpendicular to the interfaces for (a)C2OC2OC2-mim$^+$/C2OC2OC2-OSO$_3^-$ and (b)C[8]-mim$^+$/C[8]-OSO$_3^-$. This function is similar to the Z-dependent order parameter $\langle P_1(\theta)\rangle$ except that we have chosen not to normalize the function so that the actual values can be directly compared with the Z-dependent distance in Fig. 4.(Large oscillations at the edges are due to low number count and poor statistics)

more spatially diffuse. In agreement with Figs. S.4 (b), 3(b) and corresponding insets, we see from Fig. 5 that the vector projection oscillates across the full length of the slab in the case of C[8]-mim$^+$/C[8]-OSO$_3^-$ but only a single oscillation at each interface can be observed in the case of C2OC2OC2-mim$^+$/C2OC2OC2-OSO$_3^-$. This emphasizes the local vs. nonlocal effect of the interface for each of these two isoelectronic systems.

Conclusions

Significant similarities and differences exist in the structure of ILs composed of symmetric ions when these possess alkyl or isoelectronic diether tails. Both form complex alternating networks of charge and both display tail components at the vacuum interface. However, interfaces induce patterns in the liquid morphology of C[8]-mim$^+$/C[8]-OSO$_3^-$ at least across an approximately 9 nm slab. Instead, in the case of C2OC2OC2-mim$^+$/C2OC2OC2-OSO$_3^-$ the patterning effect is strictly localized at the interface. Diether tails curl, and this combined

with the more polar nature of these functionalities significantly diminishes the intermediate range order and hence the intensity of the prepeak.

Acknowledgments

This work was supported by Grant No. CHE-1362129 from the US National Science Foundation awarded to C.J.M. and No. CHE-1362272 to E.W.C.

Supporting Information

Cation head-cation head, anion head-anion head, cation head-anion head partial subcomponents of $S(q)$, table with charges, tail dihedral distributions for cation and anion in the bulk phase, bulk and slab snapshots of C[8]-mim$^+$/C[8]-OSO$_3^-$. This information is available free of charge via the Internet at http://pubs.acs.org/

References

(1) Kempter, V.; Kirchner., B. The role of hydrogen atoms in interactions involving imidazolium-based ionic liquids. *J. Mole. Struc.,* **2010**, *972*, 22–34.

(2) Sharma, S.; Gupta, A.; Kashyap., H. K. How the Structure of Pyrrolidinium Ionic Liquids Is Susceptible to High Pressure. *J. Phys. Chem. B.,* **2016**, *120*, 3206–3214.

(3) D'Angelo, P.; Serva, A.; Aquilanti, G.; Pascarelli, S.; Migliorati., V. Structural Properties and Aggregation Behavior of 1-Hexyl-3- methylimidazolium Iodide in Aqueous Solutions. *J. Phys. Chem. B.,* **2015**, *119*, 14515–14526.

(4) Triolo, A.; Russina, O.; Fazio, B.; Triolo, R.; Cola., E. D. Morphology of 1-alkyl-3-methylimidazolium hexafluorophosphate room temperature ionic liquids. *Chem. Phys. Lett.,* **2008**, *457(4)*, 362–365.

(5) Shimizu, K.; Pádua, A. A. H.; Lopes., J. N. C. Nanostructure of Trialkylmethylammonium Bistriflamide Ionic Liquids Studied by Molecular Dynamics. *J. Phys. Chem. B.,* **2010**, *114*, 1563515641.

(6) Lopes, J. N. A. C.; Padua., A. A. H. Nanostructural Organization in Ionic Liquids. *J. Phys. Chem. B.,* **2006**, *110*, 3330–3335.

(7) Morrow, T. I.; Maginn, E. J. Molecular Dynamics Study of the Ionic Liquid 1-n-Butyl-3-methylimidazolium Hexafluorophosphate. *J. Phys. Chem. B.,* **2002**, *106*, 12807–12813.

(8) Wang, Y.; Izvekov, S.; Yan, T.; Voth., G. A. Multiscale Coarse-Graining of Ionic Liquids. *J. Phys. Chem. B.,* **2006**, *110*, 3564–3575.

(9) Shimizu, K.; Bernardes, C. E. S.; Lopes., J. N. C. Structure and Aggregation in the 1-Alkyl-3-Methylimidazolium Bis(trifluoromethylsulfonyl)imide Ionic Liquid Homologous Series. *J. Phys. Chem. B.,* **2014**, *118*, 567–576.

(10) Wang, Y.; Voth., G. A. Tail Aggregation and Domain Diffusion in Ionic Liquids. *J. Phys. Chem. B.,* **2006**, *110*, 18601–18608.

(11) Popolo, M. G. D.; Voth., G. A. On the Structure and Dynamics of Ionic Liquids. *J. Phys. Chem. B.,* **2004**, *108*, 1744–1752.

(12) Kashyap, H. K.; Santos, C. S.; Murthy, N. S.; Hettige, J. J.; Kerr, K.; Ramati, S.; Gwon, J.; Gohdo, M.; Lall-Ramnarine, S. I.; Wishart, J. F. et al. Structure of 1-alkyl-1-methylpyrrolidinium bis(trifluoromethylsulfonyl)amide ionic liquids with linear, branched, and cyclic alkyl groups. *J. Phys. Chem. B.,* **2013**, *117*, 15328–15337.

(13) Kashyap, H. K.; Hettige, J. J.; Annapureddy, H. V. R.; Margulis, C. J. SAXS anti-peaks reveal the length-scales of dual positive-negative and polar-apolar ordering in room-temperature ionic liquids. *Chem. Commun.,* **2012**, *48*, 5103–5105.

(14) Hettige, J. J.; Araque, J. C.; Kashyap, H. K.; Margulis, C. J. Communication: Nanoscale structure of tetradecyltrihexylphosphonium based ionic liquids. *J. Chem. Phys.,* **2016**, *144*, 121102.

(15) Hettige, J. J.; Kashyap, H. K.; Margulis, C. J. Communication: Anomalous temperature dependence of the intermediate range order in phosphonium ionic liquids. *J. Chem. Phys.,* **2014**, *140*, 111102.

(16) Hettige, J. J.; Kashyap, H. K.; Annapureddy, H. V. R.; Margulis, C. J. Anions, the Reporters of Structure in Ionic Liquids. *J. Phys. Chem. Lett.,* **2013**, *4*, 105–110.

(17) Castner, E. W., Jr; Margulis, C. J.; Maroncelli, M.; Wishart, J. F. Ionic liquids: structure and photochemical reactions. *Annu. Rev. Phys. Chem.,* **2011**, *62*, 85–105.

(18) Araque, J. C.; Hettige, J. J.; Margulis, C. J. Ionic liquids-Conventional solvent mixtures, structurally different but dynamically similar. *J. Chem. Phys.,* **2015**, *143*, 134505.

(19) Hayes, R.; Warr, G. G.; Atkin, R. Structure and nanostructure in ionic liquids. *Chem. Rev.,* **2015**, *115*, 6357–6426.

(20) Russina, O.; Triolo., A. New experimental evidence supporting the mesoscopic segregation model in room temperature ionic liquids. *Faraday Discuss.,* **2012**, *154*, 97–109.

(21) Siqueira, L. J. A.; Ribeiro., M. C. C. Molecular Dynamics Simulation of the Ionic Liquid N-Ethyl-N,N-dimethyl-N-(2-methoxyethyl)ammonium Bis(trifluoromethanesulfonyl)imide. *J. Phys. Chem. B.,* **2007**, *111*, 11776–11785.

(22) Revelli, A.-L.; Mutelet, F.; Jaubert, J.-N.; Garcia-Martinez, M.; Sprunger, L. M.; William E. Acree, J.; Baker., G. A. Study of Ether-, Alcohol-, or Cyano-Functionalized Ionic Liquids Using Inverse Gas Chromatography. *J. Chem. Eng. Data.,* **2010**, *55*, 2434–2443.

(23) Henderson, W. A.; Victor G. Young, J.; Fox, D. M.; Longc, H. C. D.; Trulove., P. C. Alkyl vs. alkoxy chains on ionic liquid cations. *Chem. Commun.,* **2006**, 3708–3710.

(24) Smith, G. D.; Borodin, O.; Li, L.; Kim, H.; Liu, Q.; Bara, J. E.; Ginc, D. L.; Nobel., R. A comparison of ether- and alkyl-derivatized imidazolium-based room-temperature ionic liquids: a molecular dynamics simulation study. *Phys. Chem. Chem. Phys.,* **2008**, *10*, 6301–6312.

(25) Kashyap, H. K.; Santos, C. S.; Daly, R. P.; Hettige, J. J.; Murthy, N. S.; Shirota, H.; Castner, E. W., Jr.; Margulis, C. J. How Does the Ionic Liquid Organizational Landscape Change when Nonpolar Cationic Alkyl Groups Are Replaced by Polar Isoelectronic Diethers? *J. Phys. Chem. B.,* **2013**, *117*, 1130–1135.

(26) Shimizu, K.; Bernardes, C. E. S.; Triolo, A.; Lopes., J. N. C. Nano-segregation in ionic liquids: scorpions and vanishing chains. *Phys. Chem. Chem. Phys.,* **2013**, *15*, 16256–16262.

(27) Triolo, A.; Russina, O.; Caminiti, R.; Shirota, H.; Lee, H. Y.; Santos, C. S.; Murthy, N. S.; Edward W. Castner, J. Comparing intermediate range order for alkyl- vs. ether-substituted cations in ionic liquids. *Chem. Commun.,* **2012**, *48*, 49594961.

(28) Chen, Z. J.; Xue, T.; Lee., J.-M. What causes the low viscosity of ether-functionalized ionic liquids? Its dependence on the increase of free volume. *RSC. Adv.,* **2012**, *2*, 10564–10574.

(29) Siqueira, L. J. A.; Ribeiro., M. C. C. Alkoxy Chain Effect on the Viscosity of a Quaternary Ammonium Ionic Liquid: Molecular Dynamics Simulations. *J. Phys. Chem. B.,* **2009**, *113*, 10741079.

(30) Figueiredo, P. H.; Siqueira., L. J. A. The Equilibrium Structure of Lithium Salt Solutions in Ether- Functionalized Ammonium Ionic Liquids. *J. Phys. Chem. B.,* **2012**, *116*, 12319–12324.

(31) Shannon, M. S.; Tedstone, J. M.; Danielsen, S. P. O.; Hindman, M. S.; Bara., J. E. Properties and Performance of Ether-Functionalized Imidazoles as Physical Solvents for CO2 Separations. *Energy Fuels* **2013**, *27*, 3349–3357.

(32) Zhao, H.; Song, Z.; Olubajo, O.; Cowins., J. V. New Ether-Functionalized Ionic Liquids for Lipase-Catalyzed Synthesis of Biodiesel. *Appl. Biochem. Biotechnol.,* **2010**, *162*, 13–23.

(33) Nakamoto, H.; Suzuki, Y.; Shiotsuki, T.; Mizuno, F.; Higashi, S.; Takechi, K.; Asaoka, T.; Nishikoori, H.; Iba., H. Ether-functionalized ionic liquid electrolytes for lithium-air batteries. *J. Power Sources* **2013**, *243*, 19–23.

(34) Wu, T.-Y.; Su, S.-G.; Lin, K.-F.; Lin, Y.-C.; Wang, H. P.; Lin, M.-W.; Gung, S.-T.; Sun., I.-W. Voltammetric and physicochemical characterization of hydroxyl- and ether-functionalized onium bis(trifluoromethanesulfonyl)imide ionic liquids. *Electrochimica Acta* **2011**, *56*, 7278– 7287.

(35) Zhao, H.; Jones, C. L.; Cowins., J. V. Lipase dissolution and stabilization in ether-functionalized ionic liquids. *Green Chem.,* **2009**, *11*, 1128–1138.

(36) Tang, S.; Baker, G. A.; Zhao., H. Ether- and alcohol-functionalized task-specific ionic liquids: attractive properties and applications. *Chem. Soc. Rev.,* **2012**, *41*, 4030–4066.

(37) Hong, S. Y.; Im, J.; Palgunadi, J.; Lee, S. D.; Lee, J. S.; Kim, H. S.; Cheong, M.; Jung., K.-D. Ether-functionalized ionic liquids as highly efficient SO2 absorbents. *Energy Environ. Sci.,* **2011**, *4*, 1802–1806.

(38) Zubeir, L. F.; Spyriouni, T.; Roest, D.; Hill, J.-R.; Kroon., M. C. Effect of Oxygenation on Carbon Dioxide Absorption and Thermophysical Properties of Ionic Liquids: Experiments and Modeling Using Electrolyte PC-SAFT. *Ind. Eng. Chem. Res.,* **2016**, *55*, 8869–8882.

(39) Amith, W. D.; Hettige, J. J.; Castner, E. W., Jr; Margulis, C. J. Structures of Ionic Liquid Having both Anionic and Cationic Octyl Tails: Lamellar Vacuum Interface vs. Sponge-Like Bulk Order. *J. Phys. Chem. Lett.,* **2016**, *7*, 3785–3790, DOI:10.1021/acs.jpclett.6b01763.

(40) Van der Spoel, D.; Lindahl, E.; Hess, B.; Groenhof, G.; Mark, A. E.; Berendsen, H. J. C. GROMACS: Fast, flexible, and free. *J. Comput. Chem.,* **2005**, *26 (16)*, 1701–1718.

(41) Canongia Lopes, J. N.; Shimizu, K.; Pádua, A. A. H.; Umebayashi, Y.; Fukuda, S.; Fujii, K.; Ishiguro, S. A. A Tale of Two Ions: The Conformational Landscapes of Bis(trifluoromethanesulfonyl)amide and N,N-Dialkylpyrrolidinium. *J. Phys. Chem. B.,* **2008**, *112 (5)*, 1465–1472.

(42) Cornell, W. D.; Cieplak, P.; Bayly, C. I.; Gould, I. R.; Merz, K. M.; Ferguson, D. M.; Spellmeyer, D. C.; Fox, T.; Caldwell, J. W.; Kollman, P. A. A Second Generation Force Field for the Simulation of Proteins, Nucleic Acids, and Organic Molecules. *J. Am. Chem. Soc.,* **1995**, *117 (19)*, 5179–5197.

(43) McDonald, N. A.; Jorgensen, W. L. Development of an All-Atom Force Field for Heterocycles. Properties of Liquid Pyrrole, Furan, Diazoles, and Oxazoles. *J. Phys. Chem. B.,* **1998**, *102 (41)*, 8049–8059.

(44) Hess, B.; Kutzner, C.; van der Spoel, D.; Lindahl, E. Algorithms for Highly Efficient, Load-Balanced, and Scalable Molecular Simulation. *J. Chem. Theory Comput.,* **2008**, *4 (3)*, 435–447.

(45) Jorgensen, W. L.; Maxwell, D. S.; Tirado-Rives., Development and Testing of the OPLS All-Atom Force Field on Conformational Energetics and Properties of Organic Liquids. *J. Am. Chem. Soc.,* **1996**, *118 (45)*, 11225–11236.

(46) Price, M. L. P.; Ostrovsky, D.; Jorgensen, W. L. Gas-phase and liquid-state properties

of esters, nitriles, and nitro compounds with the OPLS-AA force field. *J. Comput. Chem.,* **2001**, *22 (13)*, 1340–1352.

(47) Frisch, M. J.; Trucks, G. W.; Schlegel, H. B.; Scuseria, G. E.; Robb, M. A.; Cheeseman, J. R.; Scalmani, G.; Barone, V.; Mennucci, B.; Petersson, G. A. et al. Gaussian 09 Revision E.01. Gaussian Inc. Wallingford CT 2009.

(48) Kashyap, H. K.; Margulis., C. J. Theoretical Deconstruction of the X-ray Structure Function Exposes Polarity Alternations in Room Temperature Ionic Liquids. *ECS Transactions.,* **2012**, *50 (11)*, 301–307.

(49) Kashyap, H. K.; Santos, C. S.; Annapureddy, H. V. R.; Murthy, N. S.; Margulis, C. J.; Castner, Jr., E. W. Temperature-Dependent Structure of Ionic Liquids: X-ray Scattering and Simulations. *Faraday Discuss.* **2012**, *154*, 133–143.

(50) Annapureddy, H. V. R.; Kashyap, H. K.; Biase, P. M. D.; Margulis., C. J. What is the Origin of the Prepeak in the X-ray Scattering of Imidazolium-Based Room-Temperature Ionic Liquids? *J. Phys. Chem. B.,* **2010**, *114*, 16838–16846.

(51) Nosé, S. A unified formulation of the constant temperature molecular dynamics methods. *J. Chem. Phys.,* **1984**, *81 (1)*, 511–519.

(52) Nosé, S. A molecular dynamics method for simulations in the canonical ensemble. *Mol. Phys.,* **1984**, *52 (2)*, 255–268.

(53) Parrinello, M.; Rahman, A. A new molecular dynamics method. *J. Appl. Phys.,* **1981**, *52 (12)*, 7182–7190.

(54) Darden, T.; York, D.; Pedersen, L. Particle mesh Ewald: An N log(N) method for Ewald sums in large systems. *J. Chem. Phys.,* **1993**, *98 (12)*, 10089–10092.

(55) Essmann, U.; Perera, L.; Berkowitz, M. L.; Darden, T.; Lee, H.; Pedersen, L. G. A smooth particle mesh Ewald method. *J. Chem. Phys.,* **1995**, *103 (19)*, 8577–8593.

(56) Yeh, I.-C.; Berkowitz, M. L. Ewald summation for systems with slab geometry. *J. Chem. Phys.,* **1999**, *111 (7)*, 3155–3162.

(57) Yeh, I.-C.; Wallqvist, A. On the proper calculation of electrostatic interactions in solid-supported bilayer systems. *J. Chem. Phys.,* **2011**, *134 (5)*, 055109–055109.

(58) Santos, C. S.; Annapureddy, H. V. R.; Murthy, N. S.; Kashyap, H. K.; Castner, E. W., Jr.; Margulis, C. J. Temperature-dependent structure of methyltributylammonium bis(trifluoromethylsulfonyl)amide: X ray scattering and simulations. *J. Chem. Phys.,* **2011**, *134*, 064517.

(59) Araque, J. C.; Hettige, J. J.; Margulis., C. J. Modern Room Temperature Ionic Liquids, a Simple Guide to Understanding Their Structure and How It May Relate to Dynamics. *J. Phys. Chem. B.,* **2015**, *119 (40)*, 12727–12740.

(60) Engkvist, O.; strand, P.-O.; Karlstrm, G. Intermolecular Potential for the 1,2-Dimethoxyethane-Water Complex. *J. Phys. Chem.,* **1996**, *100*, 69506957.

(61) Andersson, M.; Karlstrom, G. Conformational structure of 1,2-dimethoxyethane in water and other dipolar solvents, studied by quantum chemical, reaction field, and statistical mechanical techniques. *J. Phys. Chem.,* **1985**, *89*, 49574962.

Graphical TOC Entry

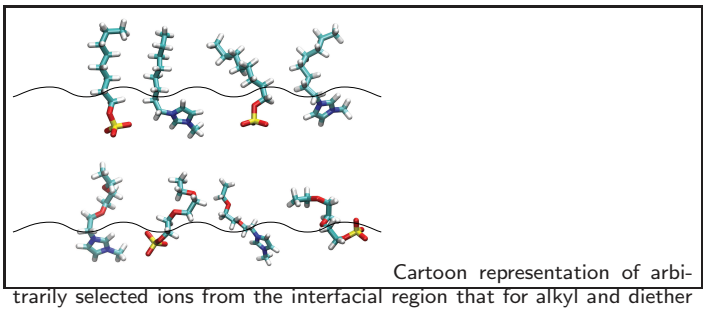

Cartoon representation of arbitrarily selected ions from the interfacial region that for alkyl and diether tails illustrate orientation and conformations.